Scattering of ^{16,18}O beams on ^{63,65}Cu targets: A systematic study of different reaction channels

V. A. B. Zagatto,[1,*] E. Crema,[1] J. M. B. Shorto,[2] M. C. Morais,[3] J. Lubian,[4] N. Added,[1] R. F. Simões,[1] D. S. Monteiro,[5] J. F. P. Huiza,[6] B. Paes,[4] and P. R. S. Gomes[4,†]

[1]*Instituto de Física da Universidade de São Paulo, 05508-090 São Paulo, Brazil*
[2]*Instituto de Pesquisas Energéticas e Nucleares, 05508-000 São Paulo, Brazil*
[3]*INFES, Universidade Federal Fluminense, Santo Antônio de Pádua, Rio de Janeiro, Brazil*
[4]*Instituto de Física da Universidade Federal Fluminense, 24210-346 Niterói, Brazil*
[5]*ILACVN, Universidade Federal da Integração Latino-Americana, 85866-000 Foz do Iguaçu, Brazil*
[6]*Universidade Estadual do Sudoeste da Bahia, Brazil*

(Received 19 June 2019; published 3 October 2019)

Precise quasielastic experimental excitation function for the $^{18}\mathrm{O} + {}^{65}\mathrm{Cu}$ system has been measured and its barrier distribution has been derived. Several reaction channels have been observed on the experimental spectra, revealing the presence of two-neutron and α-stripping processes, as well as the proton pickup transfer, for which excitation functions were also measured. Extensive coupled channel and coupled reaction channel calculations have been performed to describe the experimental data. The inelastic couplings of target and projectile, and the ground state reorientation of the target, were important to the proper description of data. The transfer data were well described by calculations; however, it was shown that they almost do not affect the excitation function of $^{18}\mathrm{O} + {}^{65}\mathrm{Cu}$ quasielastic scattering. Whenever possible, structure shell model calculations have been performed to obtain the spectroscopic amplitudes of projectile and target overlaps. The two-neutron and α-transfer reactions have been calculated considering the transferred particle as a cluster with spin 0.

DOI: 10.1103/PhysRevC.100.044602

I. INTRODUCTION

In a typical nuclear interaction, several reaction channels may be opened. Even though it is difficult to predict all the important channels that would emerge from a given scattering experiment, it is known that the elastic channel and the compound nucleus formation are always present in any nuclear reaction. The fusion process is of paramount relevance in many different contexts; for instance, it is responsible for the nucleosynthesis of elements in the interior of stars, for generating energy in nuclear power plants, and also in the quest of superheavy elements. Fusion barrier distributions (FBD) [1] have been an important tool to disentangle the reaction dynamics of several systems. Unfortunately, the technique usually presents data with high uncertainties above the Coulomb barrier. This energy region is of particular interest since relevant reaction channels become accessible.

As the total reaction cross section of any system is composed of the fusion plus the direct reaction cross sections, an alternative to performing such studies is measuring the equivalent of the FBD (at backward angles). The quasielastic barrier distribution (QEBD) method [2–5] provides the same information that FBD brings, with the benefit of increased accuracy for data taken at energies above the barrier. QEBD allows one to study important dynamical aspects of nuclear reactions, since they are extremely sensitive to the inclusion of new reaction channels in the calculations. Besides, it has been already demonstrated in Ref. [6] that the central position of the barrier is sensitive to structural information of the involved nuclei, showing that this method may provide reliable information about the interaction potential of nuclei.

Optical model (OM) potentials [7] have been widely used, among other reasons, because of the lack of computational power. Nowadays, such a theoretical approach is still being used, depending on the kind of reaction that one wants to study; for example, reactions where high excited states and resonances may be accessed [8] usually are difficult to describe theoretically. However, for reactions occurring close to the Coulomb barrier (where the number of open channels is not prohibitive), computational power is no longer an impediment to performing more complete and realistic calculations. This way, the high sensibility of QEBD method to the inclusion of different reaction channels in calculations becomes quite attractive, since the derivative of the cross sections involved in this technique usually turns subtle effects more apparent. Precise coupled channel (CC) and coupled reaction channel (CRC) calculations usually employ fewer adjustable parameters, allowing one to extract the inherent subtleties of nuclear reactions.

Many of the QEBD reactions previously measured involved only even target nuclei [9–11]. Odd nuclei are extremely important since they usually have an intrinsic nuclear deformation, which may be estimated from its quadrupole moment. Such deformations may interfere directly in the suppression or the enhancement of different nuclear channels.

*vinicius.zagatto@gmail.com
†Deceased.

A well-known example of such interference in odd nuclei is the ground-state spin reorientation effect [12–14].

In the astrophysical context, medium-mass nuclei have an important role in the stellar environment, being part of the chain of reactions which generate heavy nuclei. Even medium-mass nuclei, such as zinc [9,10], calcium, and tin [11], have already been studied. However, there is a lack of information in the literature for odd nuclei in the same mass region. Because of the easiness of manufacturing targets, copper emerges as a natural candidate to fill the experiments in this mass region. With this aim, a systematic study has been developed through the years, focusing on copper and oxygen isotopes. First, the $^{16}O + ^{63}Cu$ reaction has been measured [15] and its reaction channels characterized. To study possible reaction channels opened by the presence of two neutrons outside of the ^{16}O core, the reaction $^{18}O + ^{63}Cu$ has also been measured [16]. Then, to verify the effects of filling the $1f_{5/2}$ shell with neutrons, data on the $^{16}O + ^{65}Cu$ reaction has been acquired [17]. Finally, to complete the full study and connect or compare the different reaction channels measured with these isotopes, data on $^{18}O + ^{65}Cu$ scattering is presented in this paper.

The work is organized as it follows: In Sec. II, a brief description of the experimental setup is given; Sec. III reports the results of the previously measured systems, as well as of the present one. A qualitative discussion of data comparing systems with each other is made. The theoretical calculations performed and their compatibility with data are discussed in Sec. IV. The closing remarks and conclusion are in Sec. V.

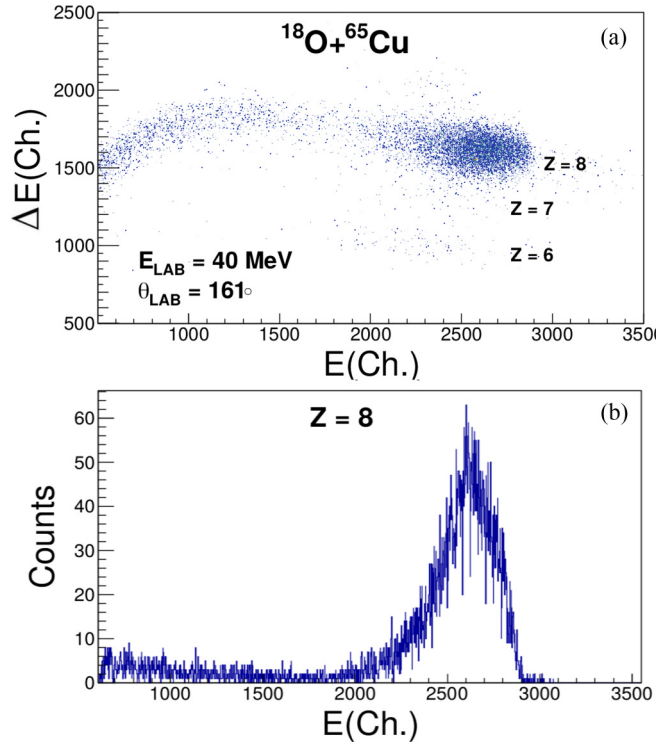

FIG. 1. (a) ΔE-E spectrum for the $^{18}O + ^{65}Cu$ reaction at 40 MeV (laboratory framework). The different Z of the reaction products are identified in the figure. (b) Typical graphical cut projection in the E axis for $Z = 8$ nuclei.

II. EXPERIMENTAL DETAILS

As the experimental setup employed to acquire the data of the reaction of the present work is similar to the ones that have already been used previously [15–17], we will present just a brief discussion of the setup and the experimental methods adopted. The data have been taken at the Pelletron 8UD accelerator of the São Paulo University. The ^{18}O beam has been delivered with energies ranging from 30 to 48 MeV (laboratory framework) with different energy steps: 1 MeV for energies far from the Coulomb barrier ($V_b = 40.1$ MeV) and 0.5 MeV for those around it. The intensities of the accelerated beam varied from 10 to 80 nA. The self-supporting isotopically enriched ^{65}Cu target (>99% purity) presented a thickness around 80 $\mu g/cm^2$.

Data have been acquired using a $\Delta E - E$ telescope detector placed at $\theta_{lab} = 161^\circ$. The telescope was composed by a ΔE proportional counter gaseous detector filled with a P-10 gas mixture at 20 Torr, plus an E surface barrier silicon detector. The scattered particles were identified in a biparametric spectrum, mainly by its charge difference [see Fig. 1(a)]. Particles with $Z = 6, 8$, and 9 are easily distinguished from each other by their differences in the ΔE axis. Eventual reactions which would result in ejectile products with the same Z value may be identified by their different loci (due to the reaction Q value) in a typical graphical cut projection in the E axis [see Fig. 1(b)].

The angular acceptance on the $\Delta E - E$ telescope has been increased to provide a higher event count rate. This allows one to perform the experiment in a reasonable time without compromising the quality of data, since we are interested in the quasielastic cross section, which is definied in Ref. [18] as the sum of elastic, inelastic, and transfer reactions cross sections. From Fig. 1(b), one may notice that the effect of increasing the angular acceptance of the experiment results is a loss of resolution on the E axis; this way, it is not possible to identify each channel individually, i.e., the quasielastic peak for $Z = 8$ represents a sum of elastic and inelastic channels, the one neutron stripping channel which has $Q = -0.979$ MeV, and some high excited states of two-neutron transfer. Once again, we reinforce that this is not a problem since the $Z = 8$ peak is quite pronounced and presents low background (<2%), which has been properly subtracted. Finally, the number of counts of each reaction is proportional to the experimental cross section, which has been normalized by data acquired in three monitor detectors placed at $\theta_{lab} = \pm 30^\circ$ and 45° (Rutherford scattering region). The experimental cross section measured for each energy will provide the excitation function (EF) of the system. Its associated QEBD may be obtained from Eq. (1) of Ref. [15], which was originally proposed in Ref. [2]. The experimental QEBD has been obtained using an energy step of 2 MeV. All the following theoretical calculations will be presented using the same energy step.

III. QUALITATIVE COMPARISON

In this section, we intend to make a qualitative comparison of the $^{18}O + ^{65}Cu$ system with those previously

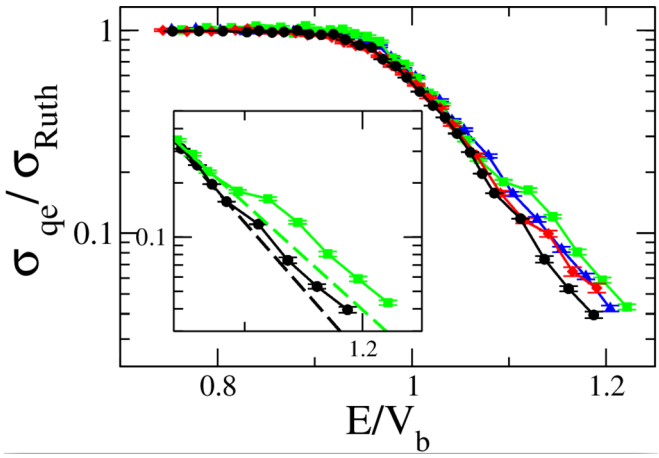

FIG. 2. EF for the four systems. The lines are just a visual guide to the eye. Data of ^{16}O + ^{63}Cu system are presented as blue triangles. ^{18}O + ^{63}Cu system is represented as red diamonds. ^{16}O + ^{65}Cu reaction data are the green squares, and the black circles correspond to ^{18}O + ^{65}Cu data. The inset in the figure is an enlargement for a better visualization of the bump.

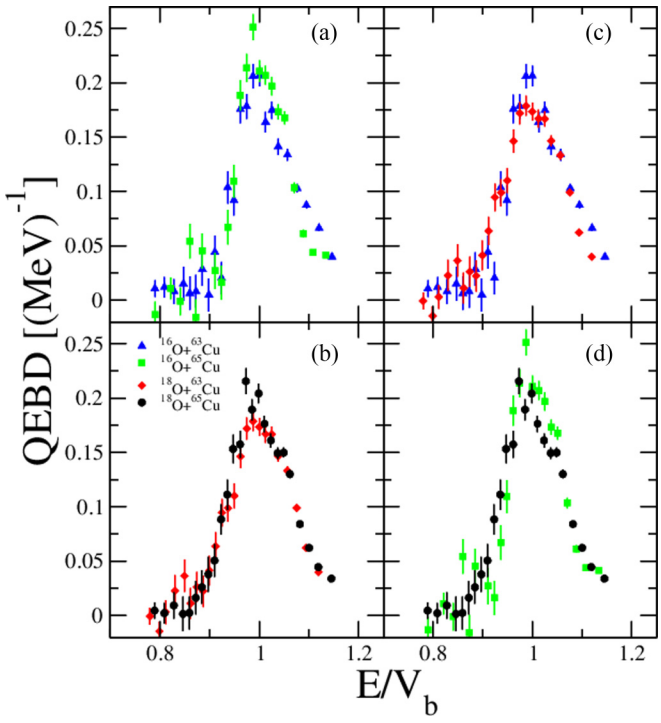

FIG. 3. QEBD for the four systems. Data of ^{16}O + ^{63}Cu system are presented as blue triangles. ^{18}O + ^{63}Cu system is represented as red diamonds. ^{16}O + ^{65}Cu reaction data are the green squares, and the black circles correspond to ^{18}O + ^{65}Cu data. The comparison is made in four panels, two systems at a time, allowing one to observe more easily the projectile and target effects.

measured (^{16,18}O + ^{63}Cu and ^{16}O + ^{65}Cu). We will discuss the observed reaction channels and also compare the shapes of the measured EF and its derived QEBD for each system. Whenever is possible, we intend to draw conclusions about the importance of a given reaction channel based on the projectile-target structure or on the previous calculations reported in Refs. [15–17]. From the qualitative comparison of the experimental spectra of these four systems, we observed that the most probable transfer channels in each reaction are determined mainly by the type of projectile. For instance, both reactions ^{16}O + ^{63,65}Cu present the α-stripping process as the most probable transfer channel, while for the ^{18}O + ^{63,65}Cu reactions, besides the α channel also the two-neutron transfer and the proton pickup seem important.

Figures 2 and 3 bring the comparison of the EF and QEBD of the four systems. The following code of shapes and colors is used to represent each system: Data of ^{16}O + ^{63}Cu system are presented as blue triangles, the ^{18}O + ^{63}Cu system is represented as red diamonds, the ^{16}O + ^{65}Cu data are the green squares, and the new data reported in this paper (^{18}O + ^{65}Cu) are represented by black circles. The lines in the EF (Fig. 2) serve as guides to the eye, not representing any fit or calculation. In order to make a proper comparison among systems, the reaction energy of data (x axis) has been normalized to the respective observed experimental Coulomb barrier energy, given by the maximum on the QEBD.

In Fig. 2, the first remarkable feature, common to most systems, is the existence of a small bump in the EF for energies above the Coulomb barrier. Since the bump occurs for $E/V_b > 1$, it is expected that such a feature is correlated to the opening of new reaction channels, which were not accessible at very low bombarding energies, and just above the barrier they present appreciable cross sections. One should notice that the amplitude of the bump, as also its position depends on each system. One may see in the figure that a possible bump occurs approximately in $E/V_b \approx 1.05$ for the ^{16}O + ^{63}Cu system; however, it is difficult to precisely evaluate it if such a feature is associated to a real bump or a statistical fluctuation of a single data point in this region. In this way, the present data do not allow one to state that there is a real bump in this system. For the other three systems, the bumps are much clearer and occur in $E/V_b \approx 1.1$. One must take into account that only a qualitative comparison of the amplitude of each bump could be done, since all data points are divided by the Rutherford cross section, which varies from one system to another and, due to the logarithmic scale adopted, the place where such bump emerges will also make it more or less visible. The bump is easily noticed for the ^{18}O + ^{63}Cu and ^{16}O + ^{65}Cu systems, being most intense for the latter case. The ^{18}O + ^{65}Cu system is the one, among these three systems, with the least perceptible bump. In order to help its visualization, the inset of Fig. 2 brings its comparison with the ^{16}O + ^{65}Cu system for energies above the barrier. An exponential decay was fitted to the data before the bump occurrence. The comparison of this fit with data helps the reader to visualize the increment in the cross section experimentally observed.

Finally, we may also observe the qualitative effects of the projectile-target combination in the QEBD (Fig. 3). Comparing the ^{16}O + ^{63}Cu and the ^{16}O + ^{65}Cu systems [Fig. 3(a)], we may infer that the peak suffers a decrease in its height due to the ^{63}Cu target. This assumption is confirmed when we compare the ^{18}O + ^{63,65}Cu systems [Fig. 3(b)] and the lower isotope generates a more flat barrier distribution. To check the

effect of the projectile, we compare the $^{16}O + ^{63}Cu$ system with the $^{18}O + ^{63}Cu$ one [Fig. 3(c)], maintaining the target and changing the projectile. The effect of the ^{18}O isotope seems to be the same as the ^{63}Cu nucleus, decreasing the height of the peak, however, in a more subtle way. This behavior is also seen when the comparison is made between $^{16,18}O + ^{65}Cu$ systems [Fig. 3(d)]. In Ref. [16], it was shown that the decrease of the distribution was mainly due to the two-neutron stripping process; however, as the projectile excitation was not considered in that paper, the present study aims to give a better understanding of the reaction mechanisms involved.

IV. THEORETICAL FRAMEWORK AND DISCUSSION

The theoretical calculations performed in the present paper intend to add new information to the previous measured systems. On the other hand, since it is also a conclusion of a systematic study performed through three different reactions, there are some constraints imposed by the preceding results. For instance, it would not be reasonable to perform nuclear structure calculations, necessary to obtain the spectroscopic amplitudes (SA) used in CRC calculations, using a different model space or nuclear interaction than those previously applied. This section will be divided into some subsections: First, the theoretical framework of the inclusion of the inelastic channels in the coupling scheme will be presented, a discussion about each transfer channel included in calculations is made individually, and, whenever needed, a brief discussion about the nuclear structure calculations is also made.

A. Inelastic channels

As demonstrated in our previous works, the inelastic channels are those with the strongest couplings and that most affect the EF and, consequently, its associated QEBD. So, a deep study of the importance of coupling each channel is once more necessary. In this work, the inclusion of the first excited states of ^{18}O (2^+ and 4^+) will be more deeply investigated. In the $^{16}O + ^{65}Cu$ reaction [17], the excited states of projectile have been shown to be of paramount importance to properly describe the measured EF and QEBD. We want to verify if this behavior is present when a different stable isotope of oxygen is used.

The theoretical framework adopted was the CC formalism and has been applied using the FRESCO code [19]. In the present calculations (and also those including transfer channels), the real nuclear potential used in the entrance channel was given by the double-folding São Paulo potential (SPP) [20–22], which has the desirable feature of having low dependence on the bombarding energy. This is required when making calculations in a wide energy range, like the one in this work. The fusion process was simulated by an imaginary inner to the Coulomb barrier Woods-Saxon potential ($V_i = 80$ MeV, $r_i = 0.8$ fm, and $a_i = 0.6$ fm), which has already been used in Refs. [15–17]. No further surface effects were taken into account by the use of any extra imaginary potential. For this reason, the transfer processes will be included via more realistic CRC calculations.

TABLE I. Spin-parity state, excitation energies (MeV), reduced matrix element (e^2 fm$^{2\lambda}$), the deformation lengths (fm), and the respective reference where these information are available for each target state included in the CC calculations.

State	E^* (MeV)	$\langle I_f \lvert E\lambda \rvert I_i\rangle$ (e^2 fm$^{2\lambda}$)	δ_λ (fm)	Ref.
$3/2^-$	Reor.	27.5	0.93	[24]
$1/2^-$	0.770	19.6	0.66	[25]
$5/2^-$	1.115	34.1	1.15	[25]
$7/2^-$	1.481	38.5	1.30	[25]
$5/2(2)^-$	1.623	9.3	0.31	[25]
$3/2(2)^-$	1.725	5.2	0.17	[25]

As the ^{18}O projectile possesses two extra neutrons when compared to its double magic ^{16}O isotope, it is expected to have a wider mass diffuseness, which would be reflected on its nuclear potential. References [6,16,23] have already demonstrated that such static effect may be considered by increasing the SPP systematic constant value of mass diffuseness of the SPP systematic from $a = 0.56$ fm to $a \approx 0.60$ fm. The same references have shown that the net effect of this correction is the displacement of the position of QEBD about 1 MeV. In our calculations, this effect has been taken into account from the beginning.

The CC calculations have been performed including the following states of target: $3/2^-$ g.s., $1/2^-$ with $E^* = 0.770$ MeV, $5/2^-$ with $E^* = 1.115$ MeV, $7/2^-$ with $E^* = 1.481$ MeV, $5/2^-$ with $E^* = 1.623$ MeV, and $3/2^-$ with $E^* = 1.725$ MeV. The ^{18}O projectile had its 0^+ g.s., 2^+ ($E^* = 1.982$ MeV), and 4^+ ($E^* = 3.555$ MeV) states incorporated in the coupling scheme. Each transition is considered in code FRESCO by its reduced matrix element, which has been obtained from the experimental values of the reduced transition probability $B(E2)\uparrow$. All the channels that have been added in the calculations are those for which such spectroscopic information is available in the literature. It is important to emphasize that the kinematical energy of these scattered particles is compatible with those that are inside the width of the $Z = 8$ peak of Fig. 1. As already been reported by Ref. [12], odd nuclei which have a permanent deformation (evaluated by its quadrupole moment) may present a reorientation effect on its g.s. Our previous works involving copper targets have shown the importance of this effect to describing the EF accurately, the EF and its QEBD. For this reason, such a component will once again be included in calculations just for the $3/2^-$ g.s. of the ^{65}Cu. A summary of the target parameters used in the CC calculations is presented in Table I.

The inclusion of each inelastic channel to calculations, how it affects the EF and its QEBD, and the comparison to experimental data may be seen in Fig. 4. Each inelastic channel has been successively added one at a time to the coupling scheme, and its effect was examined. Figures 4(a) and 4(b) show the cumulative effect after a new higher excited state of the target is added to the input. Since the inclusion of some channels did not modify the EF or the QEBD, to improve visualization, only the channels that significantly affect the cross sections are presented. One may notice from Fig. 4 that

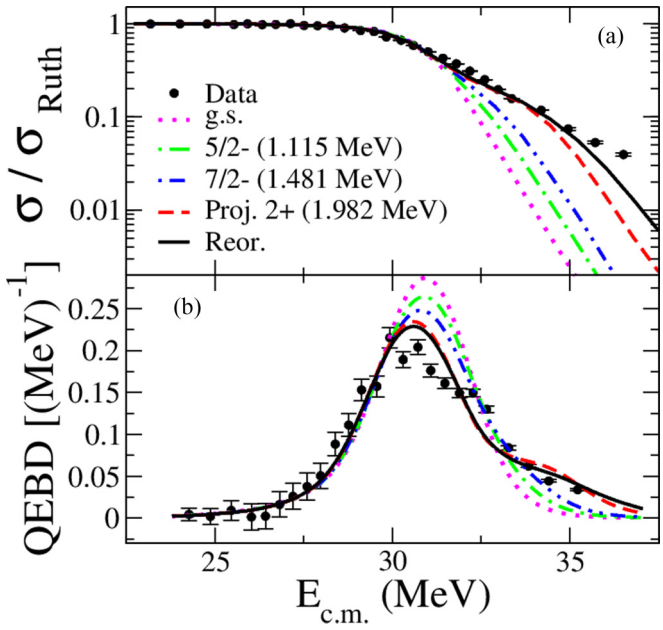

FIG. 4. (a) EF for the $^{18}O + ^{65}Cu$ system. The different lines represent CC calculations including the excited states of target, projectile, and the reorientation effect of copper g.s.; (b) QEBD for the $^{18}O + ^{65}Cu$ system.

there are just two excited states of target that strongly affect the EF and QEBD when compared to the basic optical model calculation with no couplings and no reorientation effect of the g.s. (labeled simply as "g.s." in Fig. 4): the first $5/2^-$ channel and the $7/2^-$ one. All the other inelastic excitations of the target have a negligible effect. Similar behavior is verified in the $^{16}O + ^{65}Cu$ system (Fig. 4 of Ref. [17]), indicating that it is a feature of ^{65}Cu.

The analyses of the $^{16}O + ^{63,65}Cu$ and $^{18}O + ^{63}Cu$ scatterings around the Coulomb barrier revealed the importance of the projectile states to properly describe the reaction mechanisms of that system [17]. As one should expect the same influence from the ^{18}O excitations, the same investigation was carried out here. The first two excited states of projectile (2^+ and 4^+) have been added into the coupling scheme. The respective reduced matrix element for these channels had values of 6.709 and 4.100 e^2 fm^4, calculated from the reduced transition probabilities of Refs. [26] and [27]. One should notice that the second excited state of projectile does not make a transition directly to the g.s., being an $E2$ transition to oxygen 2^+ state at $E^* = 1.982$ MeV. An analysis of Fig. 4 shows that just the first excited state of the projectile has an appreciative effect. This result is in accordance with those obtained in Ref. [17] for the ^{16}O projectile, showing that this seems to be a common effect of different oxygen isotopes. Finally, the reorientation effect is considered in the calculations and quite a good description of data is obtained. This result corroborates the relevance of the reorientation effect in copper isotopes uncovered in our previous works [15–17]. An analysis of Fig. 4(a) shows that the inclusion of the 2^+ inelastic state of the projectile is of paramount importance in the proper description of experimental data.

B. Two-neutron transfer channel

From the experimental spectrum of Fig. 1(a), the existence of counts on the energy region beyond the elastic peak position is clear. Since these events have $Z = 8$, probably they are products of the neutron-transfer processes. The ^{18}O projectile possesses two neutrons on its valence shell, and it is possible that such events are due to the one- or two-neutron transfer channels. Analyzing the respective Q values of each reaction, one would find that the one-neutron stripping process has $Q = -0.98$ MeV, while the two-neutron stripping process has $Q = 4.01$ MeV. Therefore, those observed events appear to be compatible with the two-neutron transfer reaction. The same behavior has been observed on the $^{18}O + ^{63}Cu$ reaction of Ref. [16]. Because of the high positive $Q_{g.s.}$ value of two-neutron transfer reaction, the expected kinematical loci of the experimental counts correlated to this channel will be separated from the elastic and inelastic scattering peaks (except the events with higher excitation energies). In Fig. 1(a), these separated counts are contained between channels 2900 and 3650. The calibration of this spectrum has demonstrated that the first limit is related to events with an excitation energy of approximately 2.6 MeV, while the latter is compatible with the transfer to the g.s. of target. These limits were also verified in data of other energies. So, our experimental two-neutron stripping excitation function contains only the events with total excitation energy lower than 2.6 MeV. On the other hand, the experimental EF and QEBD contain almost all events produced by all one- or two-neutron transfer reactions, regardless of the excitation energy of the reaction products. These energy limits must be adopted in calculations to make a proper comparison of it with experimental data.

The high Q value of this reaction means that the recoiling nucleus originated from the reaction (^{67}Cu) will present, according to Brink's rule [28], high excitation energies. From this point, two main problems arise: (1) Performing microscopic structural shell model calculations (to obtain the necessary spectroscopic amplitudes to CRC calculations) becomes prohibitive due to the necessity of an extremely large model space (allowing description of the low-lying and high excited states simultaneously). (2) Experimentally characterizing the resulting ^{67}Cu nucleus is difficult (just a few states have their excitation energies and spin-parity values assigned). This way, a cluster model considering the two neutrons as a structureless particle of mass 2 and spin 0 (corresponding to antiparallel coupling of its spin) coupled to the inert ^{16}O core has been adopted.

One must remember that the present data encompass all reaction products. It does not allow us to infer precise spectroscopic information about the reaction nuclei since it is impossible to distinguish the individual cross section for most of states. It does not represent in the present circumstance a limitation on the information that experimental data was expected to provide. With these inclusive data, it has been shown that it is possible to quantify the total contribution of a given channel into the EF and QEBD and assign the relevance of such channel for the reaction (which is the ultimate aim of the present work). So, the solution of adopting the cluster model to describe the two-neutron transfer process is more

than justifiable in the current situation. This procedure has been used recently to study two-neutron transfer reactions (^{18}O, ^{16}O) in several targets, like ^{12,13}C [29–31], ^{16}O [32], ^{30}Si [33], and ^{64}Ni [34]. It has been shown that when the standard value of 1.0 is used for the spectroscopic amplitudes, the two-neutron cross section gives the correct order of magnitude of the experimental data but usually overestimates them. As we do not have access to the detailed spectroscopy in the present experiment, the amplitudes will be varied to fit the experimental data.

In all CRC calculations performed in this work, the scattering potential of the final transfer partition (i.e., ^{16}O + ^{67}Cu) used as its optical potential the São Paulo systematic [35,36], where the SPP, with real and imaginary normalizations of 1 and 0.78 (respectively), is used to take into account the nuclear interaction. Such procedure effectively describes the outgoing partition, since no explicit couplings are made on them. A real Woods-Saxon potential (with adjustable depth to reproduce the binding energies) was used to bind the valence particles to its core. Such procedure has been already been proven correct and effectively describes the transfer products, as shown on Refs. [37–39]. To describe the one-neutron and one-proton transfer processes, the spin-orbit interaction has also been considered. Prior representation (considering complex remnant and nonorthogonality corrections) of the effective potential was used in our finite-range CRC calculations.

Given the inherent theoretical and experimental difficulty involving the proper energy and spin-parity assignment of ^{67}Cu nucleus, the following states have been added to the coupling scheme: $3/2^-$ g.s., $5/2^-$ ($E^* = 1.115$ MeV), $7/2^-$ ($E^* = 1.669$ MeV), $3/2(2)^-$ ($E^* = 1.937$ MeV), $7/2(2)^-$ ($E^* = 2.340$ MeV), and $3/2(3)^-$ ($E^* = 2.680$ MeV). Regarding the ^{16}O ejectile, only the 0^+ g.s. has been considered. Just transitions between the g.s. of projectile-ejectile and target-recoil have been considered. Experimental data of two-neutron transfer excitation function may be seen in Fig. 5.

From the experimental two-neutron stripping excitation function, the spectroscopic amplitudes of the CRC theoretical calculation were adjusted in order to properly describe the experiment. The same SA was used in all target-recoil overlaps, and the best fit was found when the SA was 0.55. The solid black line of Fig. 5 is the sum of all the cross sections of the previously described states of ^{67}Cu. The individual contribution of each state is also shown in the same figure. A very good agreement between experimental data and theoretical calculations is found. By analyzing the individual contribution of each state, it was found that the peak position of all states is nearly the same and the states that most seem to contribute to the total transfer cross section are both $7/2^-$. As the cross section of the $3/2(3)^-$ state abruptly declines, this may indicate that the optimum excitation energy region of the recoiling nucleus has already been accessed. Besides that, as the $7/2^-$ levels have greater cross sections than the $3/2^-$ ones, this may occur due to an angular momentum mismatch of the reaction in the latter case.

Since the two-neutron process is being properly described (by the direct comparison of transfer calculations to experimental data), we are now in a position to check how much such a reaction affects the EF and its QEBD. The comparison

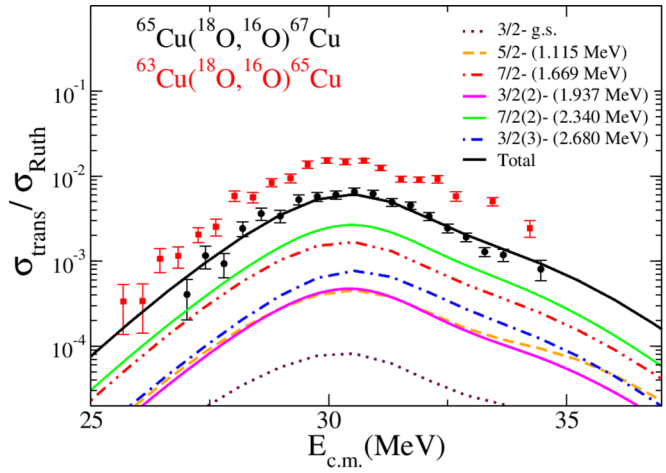

FIG. 5. Two-neutron transfer data. The calculations were performed using the overall spectroscopic amplitudes of the two-neutron transfer process set to 0.55 and are the coupling of all the states of ^{67}Cu described on the text. Each line represents the individual contribution of an excited state to the total transfer cross section (solid black line).

of theoretical cross sections with the previously presented experimental data may be seen in Fig. 6.

The inspection of Fig. 6 reveals that the EF and the QEDB are barely affected by the inclusion of the two-neutron stripping channel in the coupling scheme. As will be shown, the inclusion of all the transfer channels in CRC calculations does not have an appreciable effect on the QEBD. When comparing this result with those obtained in Ref. [16], it is revealed

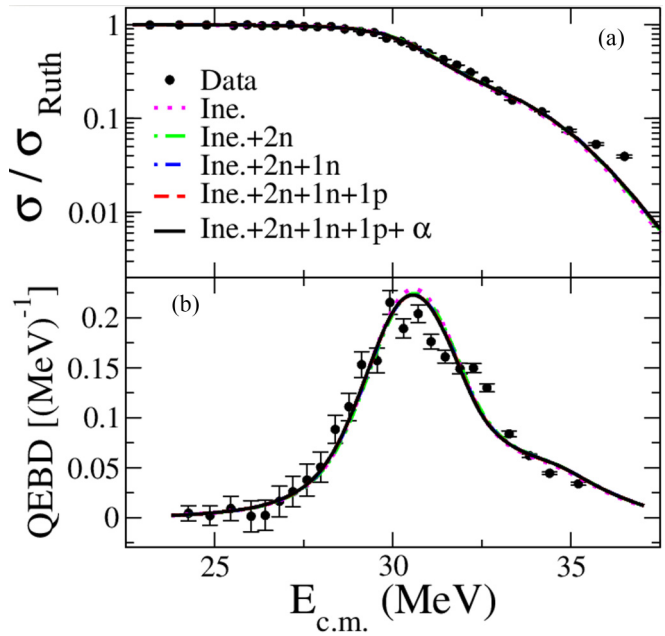

FIG. 6. (a) EF for the ^{18}O + ^{65}Cu system. The different lines represent CRC calculations including the two- and one-neutron stripping processes, the one proton pickup, and the α transfer. (b) QEBD for the ^{18}O + ^{65}Cu system.

that the two-neutron process is much more relevant in the $^{18}O + {}^{63}Cu$ reaction. In the previous reaction, the description of the EF and its QEBD is much improved by the inclusion of the two-neutron stripping. As discussed in that reference, this result (the two-neutron transfer reaction affects the EF and QEBD more than the one-neutron process) may be an indication of the existence of pairing forces between the two transferred neutrons of ^{18}O. However, one should notice that in the ^{63}Cu(^{18}O, ^{16}O)^{65}Cu reaction, the transfer cross section (shown in Fig. 5) is about three times more intense than the present case. As the projectile is the same on these both reactions and the target is the only difference, the suppression of the two-neutron transfer process in the $^{18}O + {}^{65}Cu$ system is related to the target structure.

C. One-neutron and one-proton transfer channels

Given that the procedure to obtain SA for each transfer channel is almost the same, one-neutron stripping and one-proton pickup transfer reactions will be discussed together in this subsection.

Even though the ^{65}Cu(^{18}O, ^{17}O)^{66}Cu reaction and the ^{65}Cu(^{18}O, ^{19}F)^{64}Ni may be described by similar shell model calculations (since the involved nuclei may be represented in the same model space), they have fundamental differences in their kinematical aspects. The one-neutron stripping has a $Q = -0.978$ MeV and the ^{17}O ejectile is in the same Z line of the elastically scattered ^{18}O. Therefore, the reaction products are under the quasielastic peak and it is not possible to directly measure this reaction cross section. In its turn, the ^{19}F ejectile of one-proton pickup is well distinguishable, and its experimental excitation function has been obtained. The proton-transfer reaction has a $Q = 0.541$ MeV, indicating that probably the low-lying states of ^{64}Ni recoiling nucleus will be accessed (this is also the case for the ^{66}Cu). Calculations for both reactions followed the same approach of the two-neutron case previously described. As proposed in Ref. [6], an increased ^{17}O mass diffuseness parameter was considered in the SPP.

The neutron stripping process took into account the $5/2^+$ g.s. and $1/2^+$ ($E^* = 0.870$ MeV) states of the ^{17}O ejectile. The recoiling ^{66}Cu nucleus had its 1^+ g.s., 2^+ ($E^* = 0.196$ MeV), 3^+ ($E^* = 0.275$ MeV), 1^+ ($E^* = 0.386$ MeV), 2^+ ($E^* = 0.465$ MeV), 4^+ ($E^* = 0.591$ MeV), 3^+ ($E^* = 0.729$ MeV), and 2^+ ($E^* = 0.823$ MeV) states inserted in the coupling scheme. All the transitions considered just the couplings to the g.s. of ^{18}O and ^{65}Cu nuclei, since couplings to their excited states would represent second-order transitions. The nuclear shell model calculations performed and the SA obtained will be presented soon.

The proton pickup partition considered into calculations fewer channels than the previously described reaction: the $1/2^+$ g.s., $5/2^+$ ($E^* = 0.197$ MeV), and $3/2^+$ ($E^* = 1.554$ MeV) states of ^{19}F ejectile; and the 0^+ g.s., 2^+ ($E^* = 1.346$ MeV), $2(2)^+$ ($E^* = 2.277$ MeV), and 4^+ ($E^* = 2.610$ MeV) states of ^{64}Ni. Once again, second-order transitions have been disregarded. The main features of the structure calculations performed are reported next.

The potential used to describe the interaction of the valence particle (proton or neutron) with the nuclear core to which it was bound was described by the Coulomb interaction plus the composition of a real *Woods-Saxon* potential with reduced radius $r_0 = 1.25$ fm and diffuseness $a = 0.75$ fm and a spin-orbit term (with the same geometrical parameters). Such parameters have been adopted in our previous works [16,17] and consistently have been proven to reproduce the experimental data. Further studies revealed that the diffuseness parameter does not play a central role in the description of one-particle transfer (when considering the other parameters fixed). The depth of the central *Woods-Saxon* potential was varied by code FRESCO to properly reproduce the respective experimental binding energies in each case.

1. Structure calculations

The one-neutron and one-proton SAs of the present work have been determined using the shell model code NUSHELLS [40], consisting of an independent nuclear structure calculation. Obtaining the SA from an independent and exclusively theoretical model allows one to perform more profound studies about the nuclear reaction mechanisms involved in the experiment.

However, one should always remember that the feasibility of performing such kinds of microscopic calculations depends on a series of factors: (1) the level of experimental knowledge about the nuclear structure of a given nucleus, which turns the comparison between the performed calculations and data easier; (2) the density of nuclear states per excitation energy (this way, phenomena like the inversion of two excited states are suppressed), and (3) the computational power required to perform calculations, either in the structure or reaction calculations (in this sense, one-particle transfer calculations become more feasible than the two-particles one). Given the above justifications, one may understand why the two-neutron transfer calculations (discussed in the preceding subsection) could not be performed using more fundamental or microscopic calculations (like the independent coordinates method [34]).

When performing theoretical shell model calculations, some limitations intrinsic to the model may be present. For example, a proper description of very collective states (usually present in some even-even nuclei) which proper description of excited states is just achievable taking into account the coherent movement of several nucleons. Also, the calculations present an intrinsic accuracy of some hundreds of keV in the correct description of a given state. So, energetically close levels of a nuclear excitation spectrum may appear interchanged.

The SAs for the $\langle {}^{17}O|{}^{18}O\rangle$ are already known and were originally calculated in Ref. [32]. The $\langle {}^{19}F|{}^{18}O\rangle$ overlaps have been obtained by a similar calculation, using the *p-sd* model (spanned by the $1p_{1/2}$, $1p_{3/2}$, $1d_{3/2}$, $1d_{5/2}$, and $2s_{1/2}$ orbitals) taking into consideration the filling of protons and neutrons individually. The interaction of nucleons on this orbitals of the valence subspace is usually well described by the potential proposed in Ref. [41], labeled in NUSHELLX code as psdmod, that is a modified version of the previous version for the interaction of the p and sd shells. Due to computational

TABLE II. Spectroscopic amplitudes used in the CRC calculations for one-proton and one-neutron transfer reactions. *nn*, *l*, and *j* are the quantum numbers of the proton-neutron orbitals for the reaction.

Initial	Final	*nn*	*l*	*j*	A_{lsj}
$^{18}O - 0^+$	$^{17}O - 5/2^+$	1	2	5/2	−1.279
$^{18}O - 0^+$	$^{17}O - 1/2^+$	2	0	1/2	0.455
$^{18}O - 0^+$	$^{19}F - 1/2^+$	2	0	1/2	−0.587
$^{18}O - 0^+$	$^{19}F - 5/2^+$	1	2	5/2	−0.705
$^{18}O - 0^+$	$^{19}F - 3/2^+$	1	2	3/2	0.454
$^{65}Cu - 3/2^-$	$^{66}Cu - 1(1)^+$	2	1	1/2	−0.355
$^{65}Cu - 3/2^-$	$^{66}Cu - 1(1)^+$	2	1	3/2	−0.063
$^{65}Cu - 3/2^-$	$^{66}Cu - 1(1)^+$	1	3	5/2	−0.236
$^{65}Cu - 3/2^-$	$^{66}Cu - 2(1)^+$	2	1	1/2	0.086
$^{65}Cu - 3/2^-$	$^{66}Cu - 2(1)^+$	2	1	3/2	0.056
$^{65}Cu - 3/2^-$	$^{66}Cu - 2(1)^+$	1	3	5/2	−0.617
$^{65}Cu - 3/2^-$	$^{66}Cu - 3(1)^+$	2	1	3/2	−0.054
$^{65}Cu - 3/2^-$	$^{66}Cu - 3(1)^+$	1	3	5/2	−0.706
$^{65}Cu - 3/2^-$	$^{66}Cu - 1(2)^+$	2	1	1/2	−0.438
$^{65}Cu - 3/2^-$	$^{66}Cu - 1(2)^+$	2	1	3/2	−0.237
$^{65}Cu - 3/2^-$	$^{66}Cu - 1(2)^+$	1	3	5/2	0.343
$^{65}Cu - 3/2^-$	$^{66}Cu - 2(2)^+$	2	1	1/2	0.588
$^{65}Cu - 3/2^-$	$^{66}Cu - 2(2)^+$	2	1	3/2	−0.183
$^{65}Cu - 3/2^-$	$^{66}Cu - 2(2)^+$	1	3	5/2	−0.136
$^{65}Cu - 3/2^-$	$^{66}Cu - 4(1)^+$	1	3	5/2	0.478
$^{65}Cu - 3/2^-$	$^{66}Cu - 3(2)^+$	2	1	3/2	0.050
$^{65}Cu - 3/2^-$	$^{66}Cu - 3(2)^+$	1	3	5/2	0.203
$^{65}Cu - 3/2^-$	$^{66}Cu - 2(3)^+$	2	1	1/2	−0.095
$^{65}Cu - 3/2^-$	$^{66}Cu - 2(3)^+$	2	1	3/2	−0.358
$^{65}Cu - 3/2^-$	$^{66}Cu - 2(3)^+$	1	3	5/2	0.014
$^{65}Cu - 3/2^-$	$^{64}Ni - 0(1)^+$	2	1	3/2	0.780
$^{65}Cu - 3/2^-$	$^{64}Ni - 2(1)^+$	2	1	1/2	0.285
$^{65}Cu - 3/2^-$	$^{64}Ni - 2(1)^+$	2	1	3/2	−0.390
$^{65}Cu - 3/2^-$	$^{64}Ni - 2(1)^+$	1	3	5/2	0.161
$^{65}Cu - 3/2^-$	$^{64}Ni - 2(1)^+$	1	3	7/2	0.248
$^{65}Cu - 3/2^-$	$^{64}Ni - 2(2)^+$	2	1	1/2	−0.144
$^{65}Cu - 3/2^-$	$^{64}Ni - 2(2)^+$	2	1	3/2	0.060
$^{65}Cu - 3/2^-$	$^{64}Ni - 2(2)^+$	1	3	5/2	0.021
$^{65}Cu - 3/2^-$	$^{64}Ni - 2(2)^+$	1	3	7/2	0.037
$^{65}Cu - 3/2^-$	$^{64}Ni - 4(1)^+$	1	3	5/2	0.063
$^{65}Cu - 3/2^-$	$^{64}Ni - 4(1)^+$	1	3	7/2	0.189

limitation, the number of free nucleons has been decreased and a ^{12}C core has been adopted.

The calculations for $\langle^{66}Cu|^{65}Cu\rangle$ and $\langle^{64}Ni|^{65}Cu\rangle$ were similar to those performed in Ref. [16] to obtain the $\langle^{64}Cu|^{63}Cu\rangle$ SAs. The fp model space, spanned by the $1f_{7/2}$, $2p_{3/2}$, $1f_{5/2}$, and $2p_{1/2}$ orbitals, has been adopted (considering neutrons and protons separately) with the medium interaction proposed in Ref. [42] for medium-mass nuclei in the region around nickel (called fpd6npn in NUSHELLX). As reported in Ref. [16], the computational limitations once again forced us to reduce the number of free nucleons to be sorted in this space, using as an inert core the ^{58}Ni isotope. The overlap wave functions (and their important quantum numbers) used in both calculations are presented in Table II.

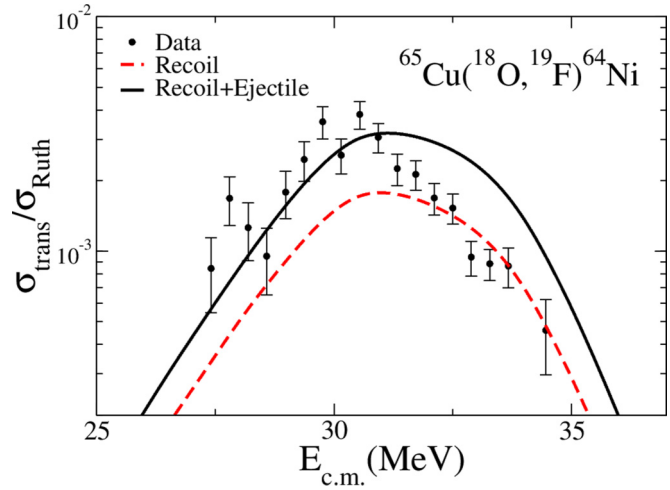

FIG. 7. Proton transfer data and its comparison with CRC calculation. The dashed red line represents the sum of the cross sections of ^{64}Ni recoil, while the solid black line also includes the transfer to states of the ^{19}F ejectile.

One may observe in Fig. 6 that both processes practically do not affect the EF and its respective QEBD. This is in accordance with the results obtained in Ref. [16], indicating that the importance of referred processes (one-neutron stripping and one-proton pickup) to the proper description of the reaction mechanism does not suffer any enhancement or suppression due to the change of the copper isotope. All the transfer channels analyzed until now marginally contribute to the description of the EF and its QEBD.

Unfortunately, as already mentioned, the data for one-neutron transfer are not available and it is not possible to investigate if the calculated SAs of Table II give an accurate measure of the existing overlaps between ^{65}Cu and ^{66}Cu nuclei. However, such inspection can be made in the proton pickup case. The comparison of CRC calculations using the SAs presented before with experimental data may be seen in Fig. 7.

The red dashed line of Fig. 7 shows the CRC calculations considering the transfer to all the previously mentioned states of ^{64}Ni recoil, disregarding any excitation in the ^{19}F ejectile. An analysis of the individual contribution of each excited state of recoiling ^{64}Ni revealed that its g.s. is responsible for almost all the observed cross section. The solid black line brings the CRC calculations that also consider the contribution from excitations of the ejectile (plus the recoil states), showing that such states have a significant contribution to the proton transfer excitation function. The calculations considering the transfer to excited states of both projectile and recoiling nuclei (solid black line) describe almost perfectly the lower energy data, while the calculations considering just the excited states of ^{64}Ni (red dashed line) described better the data measured at higher bombarding energies. We do not have an explanation for this fact. Nevertheless, the comparison to data shows that the calculated SAs can reproduce, at least, the order of magnitude of experimental cross sections, indicating that they could furnish some information to the literature.

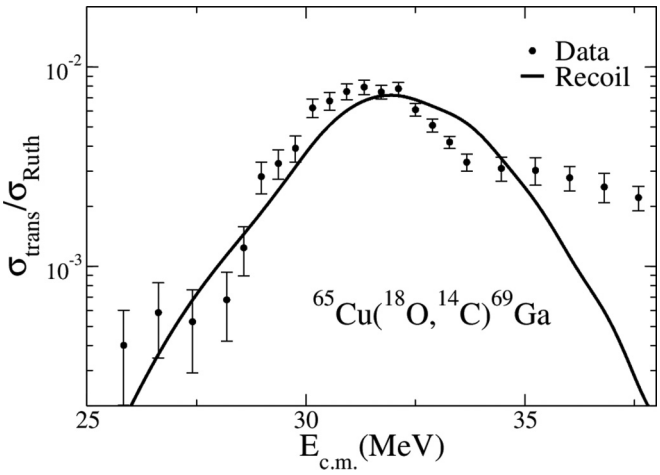

FIG. 8. α-transfer data and its comparison with CRC calculation.

D. α-particle transfer channel

The α-transfer channel is the only reaction that has been experimentally observed in all our previous works involving oxygen and copper isotopes. This is in accordance with the already known aspect of existing α clusterization on oxygen isotopes [43–49]. The data acquired throughout those works shows that this feature can also be present in other oxygen isotopes; however, more specific studies are required. One must keep in mind that it is always theoretically and experimentally hard to deal with transfer reactions. α-transfer measurements demand very specific experimental setups due to their usually low cross sections. Likewise, structural α-transfer *ab initio* calculations are very difficult to carry out.

The α-stripping SAs cannot be extracted from NushellX code. For this reason, we could only furnish an approximated description of this channel. For our aims, this is enough since we just want to inspect the importance of such a channel in the EF and QEBD. The transfer (with $Q = -1.737$ MeV) has been inserted in the CRC calculations, considering the valence α particle associated to the initially inert ^{14}C core as a spin 0 cluster. All the discussions about the CRC calculations (potentials adopted, prior representation, etc.) made before are still valid in the present case. The $3/2^-$ g.s., $7/2^-$ ($E^* = 1.337$ MeV), $7/2(2)^-$ ($E^* = 1.488$ MeV), $3/2(2)^-$ ($E^* = 1.526$ MeV), $5/2^-$ ($E^* = 1.724$ MeV), $9/2^-$ ($E^* = 1.765$ MeV), $3/2(3)^-$ ($E^* = 1.892$ MeV), and $7/2(3)^-$ ($E^* = 1.924$ MeV) states of ^{69}Ga have been added to the coupling scheme, as also the 0^+ g.s., 1^- ($E^* = 6.094$ MeV), and 3^- ($E^* = 6.728$ MeV) states of ^{14}C. Our aim in including the excited states of ejectile was to verify if the same behavior noted in the ^{65}Cu(^{16}O, ^{12}C)^{69}Ga reaction [17], where the excitation of ejectile was important to describe the observed transfer excitation function in higher energies, is also present for the ^{18}O + ^{65}Cu system. Figure 8 presents the comparison of theoretical CRC calculations and experimental data.

The SAs of CRC overlaps have been adjusted to provide the best possible accord to experimental data. The adjusted SAs of target-recoil overlaps had the same value for each transition and the best accord was found when the SA was 0.3. From Fig. 8, one may see that data for energies up to 35 MeV are well described. The transitions for $\langle^{14}\text{C}|^{18}\text{O}\rangle$ overlaps (with SAs set to unity) have considerable cross sections just in the region above 33 MeV, also presenting a prominent bell shape, not describing precisely the experimental data. There are many possibilities that could explain the disagreement of data and theoretical calculations, like the necessity of including more excited states (of ejectile and recoil) in the coupling scheme or even the possibility that, at such high reaction energies, other reaction mechanisms may occur. Reference [50] has shown that in the ^{18}O + ^{174}Yb system, correlated multinucleon transfer may occur, resulting in several carbon isotopes ejectiles. An analysis of Figs. 3, 4, and 6 of this reference shows that the ^{14}C isotope is the one with higher cross section; however, the ^{12,13,15}C isotopes have also a not insignificant contribution. With the detection apparatus employed in our measurements, it is not possible to separate the individual contribution of each isotope. The theoretical treatment of multinucleon transfer resulting in other carbon isotopes is beyond the scope of this work. As reported in our previous works, the inclusion of the α-transfer channel does not affect the EF and its QEBD (as may be seen in Fig. 6).

V. CONCLUSIONS

The ^{16}O + ^{63}Cu [15], ^{18}O + ^{63}Cu [16], ^{16}O + ^{65}Cu [17], and ^{18}O + ^{65}Cu (present work) precise EF (also their respective QEBD) have been measured and its reaction channels studied. The present work has performed a systematic qualitative comparison of all these systems, focusing mainly on the unpublished ^{18}O + ^{65}Cu reaction data. From this comparison, many different features have been observed and several conclusions have been drawn. It was observed that the α-transfer stripping reaction had been observed in all of the four reactions, reinforcing the common description of oxygen isotopes as a cluster of α particles. However, even being always present, the inclusion of such a reaction channel in the CRC coupling scheme does not affect the EF and QEBD. It was also noticed from the experimental spectra that, whenever the ^{18}O projectile is present, further transfer reaction channels are observed, including the two-neutron transfer and the proton pickup. A comparative analysis of experimental EF and QEBD revealed that either the ^{18}O or the ^{63}Cu presence have similar effects, causing a faster decrease of the EF at energies around the barrier and a suppression of the main peak of the QEBD. Another general feature which is present in most systems is the existence of a small bump in the EF at energies above the Coulomb barrier. In Ref. [17], it was possible to associate it to the coupling of high excited states of the projectile into calculations.

As for the ^{18}O + ^{65}Cu system, it was demonstrated in this paper that the experimental EF and its respective QEBD are theoretically well described mainly by the presence of inelastic excitations of target and projectile. The CC calculations here performed have demonstrated that the first $5/2^-$ and the $7/2^-$ excited states of ^{65}Cu are the two channels that most strongly affect the EF and QEBD description. Besides them, the reorientation effect of the $3/2^-$ g.s. of the target is once again very important. Based on the results of Ref. [17], the inelastic channels of projectile have been incorporated in

calculations. The 2^+ state of ^{18}O has demonstrated paramount importance in the description of EF and QEBD, indicating that it is a common feature in oxygen isotopes. The inclusion of the inelastic states describes well the experimental data.

Several transfer reaction mechanisms have been incorporated into calculations by the CRC method. The inclusion of all the transfer channels hardly affected the theoretical EF and QEBD. This was expected since the inclusion of the inelastic channels gave a good fit to data. Usually, the inelastic excitations are associated with collective motions of some nucleons, while the transfer of particles is a peripheral process involving few valence particles. Therefore, the theoretical calculations here performed, indicating the prevalence of inelastic channels over the transfer ones, may indicate that collective motions affect the reaction cross section more than the individual ones. The two-neutron transfer, the proton pickup, and the α-stripping channels had their excitation functions acquired. The CRC calculations performed here gave a good description of the experimental data. One-neutron transfer has also been incorporated into calculations, although this event is indistinguishable from the experimental quasielastic peak. The single-neutron and proton SAs have been obtained via nuclear shell model calculations with NUSHELLX code. The comparison of proton data with CRC calculations indicates that the structure calculations provided spectroscopic information that, at least, seems to give the correct order of magnitude of the initial-final wave function overlaps. However, one must always remember the limitations (discussed in the text) of the present experiment in providing such kind of information. The α and two-neutron transfers were considered in calculations using a cluster model. Both excitation functions were well described by calculations.

ACKNOWLEDGMENTS

This work was partially supported by FAPESP, FAPERJ, CAPES, CNPq, and INCT-FNA (Instituto Nacional de Ciência e Tecnologia-Física Nuclear e Aplicações) (Proc. No. 464898/2014-5). We would also like to thank the technical staff of LAFN for assisting in the maintenance and operation of the accelerator.

[1] N. Rowley, G. R. Satchler, and P. H. Stelson, Phys. Lett. B **254**, 25 (1991).
[2] H. Timmers, J. R. Leigh, M. Dasgupta, D. J. Hinde, J. C. Lemmon, J. C. Mein, C. R. Morton, J. O. Newton, and N. Rowley, Nucl. Phys. A **584**, 190 (1995).
[3] N. Rowley, H. Timmers, J. R. Leigh, M. Dasgupta, D. J. Hinde, J. C. Mein, C. R. Morton, and J. O. Newton, Phys. Lett. B **373**, 23 (1996).
[4] H. Timmers, D. Ackermann, S. Beghini, L. Corradi, J. H. He, G. Montagnoli, F. Scarlassara, A. M. Stefanini, and N. Rowley, Nucl. Phys. A **633**, 421 (1998).
[5] R. F. Simões, D. S. R. Monteiro, J. M. B. Shorto, A. M. Jacob, L. K. Ono, E. Crema, and N. Added, Phys. Lett. B **527**, 187 (2002).
[6] E. Crema, D. R. Otomar, R. F. Simoes, A. Barioni, D. S. Monteiro, L. K. Ono, J. M. B. Shorto, J. Lubian, and P. R. S. Gomes, Phys. Rev. C **84**, 024601 (2011).
[7] C. M. Perey and F. G. Perey, At. Data Nucl. Data Tables **17**, 1 (1976).
[8] V. A. B. Zagatto, F. Cappuzzello, J. Lubian, M. Cavallaro, R. Linares, D. Carbone, C. Agodi, A. Foti, S. Tudisco, J. S. Wang, J. R. B. Oliveira, and M. S. Hussein, Phys. Rev. C **97**, 054608 (2018).
[9] J. F. P. Huiza, E. Crema, D. S. Monteiro, J. M. B. Shorto, R. F. Simoes, N. Added, and P. R. S. Gomes, Phys. Rev. C **75**, 064601 (2007).
[10] J. F. P. Huiza, E. Crema, A. Barioni, D. S. Monteiro, J. M. B. Shorto, R. F. Simoes, and P. R. S. Gomes, Phys. Rev. C **82**, 054603 (2010).
[11] E. Crema, M. A. G. Alvarez, N. H. Medina, L. R. Gasques, J. F. P. Huiza, B. Fernandez, Z. Abou-Haidar, P. N. de Faria, P. R. S. Gomes, J. Lubian, and D. Verney, Phys. Rev. C **88**, 044616 (2013).
[12] G. R. Satchler, Nucl. Phys. A **45**, 197 (1963).
[13] S. E. Hicks and M. T. McEllistrem, Nucl. Phys. A **468**, 372 (1987).
[14] V. Hnizdo, K. W. Kemper, and J. Szymakowski, Phys. Rev. Lett. **46**, 590 (1981).
[15] J. M. B. Shorto, E. Crema, R. F. Simoes, D. S. Monteiro, J. F. P. Huiza, N. Added, and P. R. S. Gomes, Phys. Rev. C **78**, 064610 (2008).
[16] E. Crema, V. A. B. Zagatto, J. M. B. Shorto, B. Paes, J. Lubian, R. F. Simoes, D. S. Monteiro, J. F. P. Huiza, N. Added, M. C. Morais, and P. R. S. Gomes, Phys. Rev. C **98**, 044614 (2018).
[17] E. Crema, V. A. B. Zagatto, J. M. B. Shorto, B. Paes, J. Lubian, R. F. Simoes, D. S. Monteiro, J. F. P. Huiza, N. Added, M. C. Morais, and P. R. S. Gomes, Phys. Rev. C **99**, 054623 (2019).
[18] K. Hagino and N. Rowley, Braz. J. Phys. **35**, 890 (2005).
[19] I. J. Thompson, Comp. Phys. Rep. **7**, 167 (1988).
[20] M. A. Candido Ribeiro, L. C. Chamon, D. Pereira, M. S. Hussein, and D. Galetti, Phys. Rev. Lett. **78**, 3270 (1997).
[21] L. C. Chamon, D. Pereira, M. S. Hussein, M. A. Candido Ribeiro, and D. Galetti, Phys. Rev. Lett. **79**, 5218 (1997).
[22] L. C. Chamon, B. V. Carlson, L. R. Gasques, D. Pereira, C. De Conti, M. A. G. Alvarez, M. S. Hussein, M. A. Cândido Ribeiro, E. S. Rossi, Jr., and C. P. Silva, Phys. Rev. C **66**, 014610 (2002).
[23] D. Pereira, C. P. Silva, J. Lubian, E. S. Rossi Jr., L. C. Chamon, G. P. A. Nobre, and T. Correa, Nucl. Phys. A **826**, 211 (2009).
[24] N. J. Stone, At. Data Nucl. Data Tables **90**, 75 (2005).
[25] E. Browne and J. K. Tuli, Nuc. Data Sheets **111**, 2425 (2010).
[26] S. Raman, C. W. Nestor, and P. Tikkanen, At. Data Nucl. Data Tables **78**, 1 (2001).
[27] https://www.nndc.bnl.gov/ensdf
[28] D. M. Brink, Phys. Lett. B **40**, 37 (1972).
[29] M. Cavallaro, F. Cappuzzello, M. Bondi, D. Carbone, V. N. Garcia, A. Gargano, S. M. Lenzi, J. Lubian, C. Agodi, F. Azaiez *et al.*, Phys. Rev. C **88**, 054601 (2013).
[30] F. Cappuzzello, D. Carbone, M. Cavallaro, M. Bond, C. Agodi, F. Azaiez, A. Bonaccorso, A. Cunsolo, L. Fortunato, A. Foti *et al.*, Nat. Commun. **6**, 6743 (2015).

[31] D. Carbone, J. L. Ferreira, F. Cappuzzello, J. Lubian, C. Agodi, M. Cavallaro, A. Foti, A. Gargano, S. M. Lenzi, R. Linares, and G. Santagati, Phys. Rev. C **95**, 034603 (2017).
[32] M. J. Ermamatov, F. Cappuzzello, J. Lubian, M. Cubero, C. Agodi, D. Carbone, M. Cavallaro, J. L. Ferreira, A. Foti, V. N. Garcia *et al.*, Phys. Rev. C **94**, 024610 (2016).
[33] E. N. Cardozo, J. Lubian, R. Linares, F. Cappuzzello, D. Carbone, M. Cavallaro, J. L. Ferreira, A. Gargano, B. Paes, and G. Santagati, Phys. Rev. C **97**, 064611 (2018).
[34] B. Paes, G. Santagati, R. M. Vsevolodovna, F. Cappuzzello, D. Carbone, E. N. Cardozo, M. Cavallaro, H. Garcia-Tecocoatzi, A. Gargano, J. L. Ferreira *et al.*, Phys. Rev. C **96**, 044612 (2017).
[35] M. A. G. Alvarez, L. C. Chamon, M. S. Hussein, D. Pereira *et al.*, Nuc. Phys. A **723**, 93 (2003).
[36] L. R. Gasques, L. C. Chamon, P. R. S. Gomes, and J. Lubian, Nucl. Phys. A **764**, 135 (2006).
[37] V. A. B. Zagatto, J. Lubian, L. R. Gasques, M. A. G. Alvarez, L. C. Chamon, J. R. B. Oliveira, J. A. Alcantara-Nunez, N. H. Medina, V. Scarduelli, A. Freitas *et al.*, Phys. Rev. C **95**, 064614 (2017).
[38] V. A. B. Zagatto, J. R. B. de Oliveira, L. R. Gasques, J. Alcantara-Nunez *et al.*, J. Phys. G **43**, 055103 (2016).
[39] L. R. Gasques, A. S. Freitas, L. C. Chamon, J. R. B. Oliveira, N. H. Medina, V. Scarduelli, E. S. Rossi Jr., M. A. G. Alvarez, V. A. B. Zagatto, J. Lubian *et al.*, Phys. Rev. C **97**, 034629 (2018).
[40] B. A. Brown and W. D. M. Rae, Nucl. Data Sheets **120**, 115 (2014).
[41] Y. Utsuno and S. Chiba, Phys. Rev. C **83**, 021301(R) (2011).
[42] W. A. Richter, M. G. van der Merwe *et al.*, Nucl. Phys. A **523**, 325 (1991).
[43] M. R. D. Rodrigues, T. Borello-Lewin, H. Miyake, F. Cappuzzello, M. Cavallaro, J. L. M. Duarte, C. L. Rodrigues, M. A. de Souza, L. B. Horodynski-Matsushigue, A. Cunsolo *et al.*, EPJ Web Conf. **66**, 02093 (2014).
[44] M. R. D. Rodrigues, T. Borello-Lewin, H. Miyake, J. L. M. Duarte, C. L. Rodrigues, M. A. Souza, L. B. Horodynski-Matsushigue, G. M. Ukita, F. Cappuzzello, A. Cunsolo *et al.*, Phys. Rev. C **89**, 024306 (2014).
[45] I. Weitzenfelder, N. Bischof, W. Tiereth, H. Voit, W. von Oertzen, and H. H. Wolter, Nucl. Phys. A **489**, 125 (1988).
[46] S. Hamada, N. Burtebayev, K. A. Gridnev, and N. Amangeldi, Nucl. Phys. A **859**, 29 (2011).
[47] W. von Oertzen and H. G. Bohlen, Phys. Rep. **19**, 1 (1975).
[48] Y. Suzuki, Prog. Theor. Phys. **55**, 1751 (1976).
[49] J. L. Ferreira, J. Lubian, R. Linares, M. J. Ermamatov, H. Yepez-Martinez, and P. O. Hess, Eur. Phys. J. A **55**, 94 (2019).
[50] P. K. Sahu, R. K. Choudhury, D. C. Biswas, and B. K. Nayak, Phys. Rev. C **64**, 014609 (2001).